# Unveiling the Effects of Machining Parameters on Material Removal Rate, Surface Roughness, and White Layer Formation in Hardened Steel

Mohd Aidil Shah bin Abdul Rahim<sup>1\*</sup>, Saifuldin bin Sabdin<sup>2</sup>

<sup>1</sup>Tool Department (Die), Proton Institute @ Advance Training Center (ADTEC) Melaka, 78000 Alor Gajah, Melaka, Malaysia

<sup>2</sup>Metal Fabrication Department, Advance Training Center (ADTEC), Tangkak Campus, Km 43, Jalan Segamat, Sagil, 84900 Tangkak, Malaysia

\* Corresponding author e-mail address: aidilshah@jtm.gov.my

**ABSTRACT:** This study investigates the impact of Wire Electrical Discharge Machining (WEDM) parameters on Material Removal Rate (MRR), Surface Roughness (SR), and White Layer Thickness (WLT) in hardened tool steel, particularly focusing on enhanced XW42 steel variants. A two-level full factorial design (FFD) and Analysis of Variance (ANOVA) were used to examine the influence of pulse-on time (T<sub>on</sub>), voltage (V), and wire tension (WT) on machining performance. Among the modified steels, enhanced XW42 (M3)—enhanced with cerium (Ce), lanthanum (La), and niobium (Nb)—exhibited superior machinability. Enhanced XW42 (M3) demonstrated the lowest WLT (144.32μm) and SR (1.92μm) under optimized conditions (T<sub>on</sub>: 2μs, V: 6V, WT: 120N), along with a high MRR of 0.00811kg/s. SEM and EDS analyses confirmed the formation of a smooth recast layer with minimal defects such as cracks, voids, and residual debris, indicating stable machining. The presence of cerium and lanthanum contributed to grain refinement and enhanced thermal stability, while niobium improved hardness and resistance to white layer formation. Predictive modelling for enhanced XW42 (M3) further validated the machining response trends, confirming its suitability for precise process optimization. Regression models showed strong predictive accuracy with R<sup>2</sup> values exceeding 93% for SR and WLT, and low average errors (SR: 0.7%, WLT: 8.2%). Voltage was identified as the most significant factor affecting WLT (69.23%), whereas Ton had the highest influence on SR (64.45%). These findings underscore the importance of alloying elements and optimized WEDM parameters in achieving high-performance surface integrity and machining efficiency, particularly for applications in the tool and die industry.

Keywords: Cerium, Niobium, Material Removal Rate, WEDM, White Layer Thickness

#### 1.0 INTRODUCTION

Wire Electrical Discharge Machining (WEDM) has emerged as a pivotal technique for machining hard steel components, especially those with hardness exceeding 50 HRC (Ndaliman, 2022). Its precision and efficiency make it indispensable in the manufacturing of dies and molds (Rosli, Jamaludin, & Azuddin, 2018). To withstand the high thermal and mechanical stresses during machining, advanced tool steels like enhanced XW42 have been developed. XW42, known for its high wear resistance and moderate toughness, is widely utilized in applications such as blanking, cutting, and forming operations, particularly in medium to large production molds (Rosli et al., 2018). In WEDM, critical output responses include Surface Roughness (SR), White Layer Thickness (WLT), and Material Removal Rate (MRR). The white layer, formed due to rapid solidification, often contains micro-cracks that compromise fatigue strength and mechanical reliability (Kumar et al., 2022; Singh & Rao, 2023). Surfaces with thick or micro-cracked white layers are unsuitable for high-temperature or cyclic loading applications. Likewise, MRR reflects the efficiency of material removal and significantly impacts overall machining productivity. However, increasing MRR often comes at the expense of surface integrity and dimensional accuracy, highlighting the need for optimized parameter selection (Arif et al.,

2022; Yadav et al., 2023).

Surface integrity, particularly expressed through SR and WLT, directly influences functional performance, including fatigue life, corrosion resistance, creep durability, and tribological behavior. The formation of the white layer typically leads to deterioration in these properties, necessitating advanced alloy development and precise control of machining parameters to mitigate its presence (Kumar et al., 2022; Yadav et al., 2023). MRR, as a measure of productivity, must also be balanced with these integrity factors to achieve optimal performance in industrial applications.

Much of the current literature on hard machining is centered on AISI D2, typically using conventional methods such as milling and turning. For instance, high-speed dry milling of AISI D2 hardened to 52 HRC has been explored (Das & Sahoo, 2023), and neural networks have been employed to predict tool wear and SR during milling (Kumar & Verma, 2020). Other studies have evaluated force analysis and surface quality during the turning of EN X160CrMoV12, and investigations into coatings and tool performance during hard turning have also been carried out (Kumar & Verma, 2020).

Longer pulse-off times and increased gap voltage have been demonstrated to reduce SR (Kumar et al., 2022), while shorter pulse-on durations can enhance MRR albeit with trade-offs in SR and WLT (Yadav et al., 2023). Optimization approaches such as grey relational analysis, response surface methodology (RSM), and machine learning models have been employed to balance multiple responses—MRR, SR, kerf width, and dimensional precision—on various materials including tool steels, aluminum matrix composites, and stainless steels (Arif et al., 2022; Zhang et al., 2024).

While past studies have used methods like RSM and ANN to predict WEDM performance, these models often face challenges in capturing nonlinear interactions or require large datasets (Kumar & Verma, 2020; Das & Sahoo, 2023). Additionally, most prior research focuses on conventional steels, limiting their accuracy when applied to advanced materials like XW42. Therefore, a more reliable and adaptable predictive model is needed to accurately correlate machining parameters with SR, WLT, and MRR for enhanced tool steel applications.

# Therefore, this study aims to:

1. Investigate the influence of WEDM parameters on SR, WLT, and MRR of enhanced XW42 tool steel; and

2. Develop predictive models to determine optimal machining conditions for improved productivity and surface integrity in precision die and mold applications.

## 2.0 METHODOLOGY

Both the original and enhanced cold work tool steels were machined to dimensions of 20mm  $\times$  10mm  $\times$  10mm for the experimental procedures. The dependent variables in this study are surface roughness (SR), material removal rate (MRR), and white layer thickness (WLT), while the independent variables are pulse-on time ( $T_{on}$ ), gap voltage (V), and wire tension, as referenced by Yadav et al. (2023) and Zhang et al. (2024). The alloying elements added to the enhanced cold work tool steel were based on standardized composition ranges, as detailed in Table 1.

Table 1: Alloy element added to the XW42 base compositions (g)

Element	С	Si	Mn	P	S	Cr	Mo	Ni
XW42	-	-	-	-	-	-	-	-
<b>M1</b>	5.8	-	-	-	-	7.5	0.2	1.5
<b>M2</b>	8.6	-	-	-	-	18.4	2.5	1.6
<b>M3</b>	12.7	-	-	-	-	5.1	4.9	1.5
Element	Cu	W	V	Nb	Ce/La	Co	Ti	Fe
XW42	-	-	-	-	-	-	-	-
<b>M1</b>	-	1.3	0.2	-	-	-	-	-
<b>M2</b>	-	2.1	1.9	1.3	0.2	-	0.1	-
M3	-	2.9	5.4	5.2	0.6	-	0.3	-

Standard base composition of Assab XW-42 (AISI D2) tool steel: 1.55 %C, 0.30 % Si, 0.40 % Mn, 11.3–12.0 % Cr, 0.80 % Mo, 0.90 % V.

## 2.1 Machine used

A numerically controlled WEDM machine, Sodick AG600L5s, was utilized in this study (Sodick, 2020). The machine is located at the Advanced Training Centre, Alor Gajah, Melaka. It operates by feeding the electrode wire at a constant speed while simultaneously supplying current through the wire (Zhang & Zhang, 2019). One of the advanced features of this model is its automatic adjustment of wire tension and speed, which helps prevent machine failure due to wire rupture (Tan, 2021). A 0.20 mm diameter brass wire was employed as the electrode, and de-ionized water was used as the dielectric fluid, supplied from both the upper and lower nozzles (Kumar et al., 2020).

A custom-designed fixture was employed to securely hold the prismatic workpiece during machining (Figure 1). Due to the small dimensions of the specimens (10mm × 10mm × 20mm), meticulous setup was necessary to ensure accurate vertical alignment within the fixture (Smith & Lee, 2018). Machining conditions were selected based on the manufacturer's specifications and operational recommendations (Sodick, 2020). The primary response variables considered in the experiment were Material Removal Rate (MRR), Surface Roughness (SR), and White Layer Thickness (WLT) (Yuan

& Zhou, 2021). The machine settings for constant parameters used throughout the experiments are summarized in Table 2.



Figure 1: A custom-designed fixture to securely hold the prismatic workpiece during machining

Table 2: Constant machining parameters

Machining parameters	Value
Pulse off time	7 ~ 50
Spark gap set voltage	10V ~ 75V
Flush pressure	0 ~ 7 psi
Feed rate	$0 \sim 50 \text{ mm/s}$
Wire feed	5-340  mm/s
Main power supply voltage	34V

Sodick, 2020

These parameters were kept constant throughout all trials, while selected process variables ( $T_{on}$ , V, and wire tension) were varied systematically to assess their impact on the defined response characteristics (MRR, SR, and WLT) (Tan & Zhang, 2019).

# 2.2 Experimental design

The objective of this research is to examine the performance of Wire Electrical Discharge Machining (WEDM) parameters, specifically focusing on Material Removal Rate (MRR), White Layer Thickness (WLT), and Surface Roughness (SR). To evaluate how various machining parameters influence these responses, a structured experimental procedure was conducted using a range of selected input values designed for this study.

All experiments were performed using a Sodick AG600L WEDM machine (Sodick, 2020). Previous works by Gautier et al. (2015) have demonstrated the applicability of full factorial design (FFD) in WEDM investigations. The design of experiments followed a  $2^k$  full factorial design (FFD) without replication, where k=3, resulting in 8 experimental runs plus 4 center points, totaling 12

experimental runs per sample. The selected low, middle, and high levels of each input variable were derived from the machine manufacturer's manual and are presented in Table 3.

Table 3: Levels of responses chosen for experiment

Pulse On Time (Ton; µs)	Voltage (V; V)	Wire Tension (WT; N)	
2	6	80	
6	8	100	
8	10	120	
8	10		

Sodick, 2020

All experiments were conducted based on a two-level factorial experimental design, and results were collected for the three machining responses: MRR, SR, and WLT. Data analysis, visualization, and model development were performed using Design Expert software (Stat-Ease, 2020). In general, lower surface roughness values are indicative of better surface finish and higher machining performance, while higher MRR and WLT values indicate higher productivity and potential surface compromise, respectively (Zhang & Zhang, 2019).

#### 3.0 DATA ANALYSIS AND FINDINGS

This chapter presents the final findings related to the alloy compositions, metallurgical analyses, and mechanical properties of both annealed and tempered steels, specifically XW42, M1, M2, and enhanced XW42 (M3). Detailed characterization includes microstructural evaluation, hardness testing, and fractography analysis to understand the influence of heat treatment on the material behavior. In addition, the machinability of these tool steels was investigated using a two-level full factorial design (DoE), considering three key machining parameters: pulse-on time (Ton), voltage (V), and wire tension (WT). The study evaluates their impact on surface roughness (SR), material removal rate (MRR), and white layer thickness (WLT) to determine the optimal machining performance across different material conditions.

## 3.1 Scanning Electron Microscope (SEM)/Energy Dispersive Spectroscopy

(EDS) investigation on white layer thickness

Figure 2(a) illustrates Sample 5 from XW42, exhibiting a white layer thickness of  $185.3 \pm 5.26 \mu m$  under the machining parameters of  $T_{on}$ :  $2\mu s$ , V: 10V, and WT: 80N. Figure 2(b) displays Sample 6 from the M1 alloy, which exhibited the thinnest white layer among the studied samples, with a thickness of  $152.8 \pm 3.69 \mu m$ , achieved at  $T_{on}$ :  $2\mu s$ , V: 6V, and WT: 120N. As expected, a lower voltage resulted in reduced thermal input during machining, thereby decreasing the extent of the white layer formation.

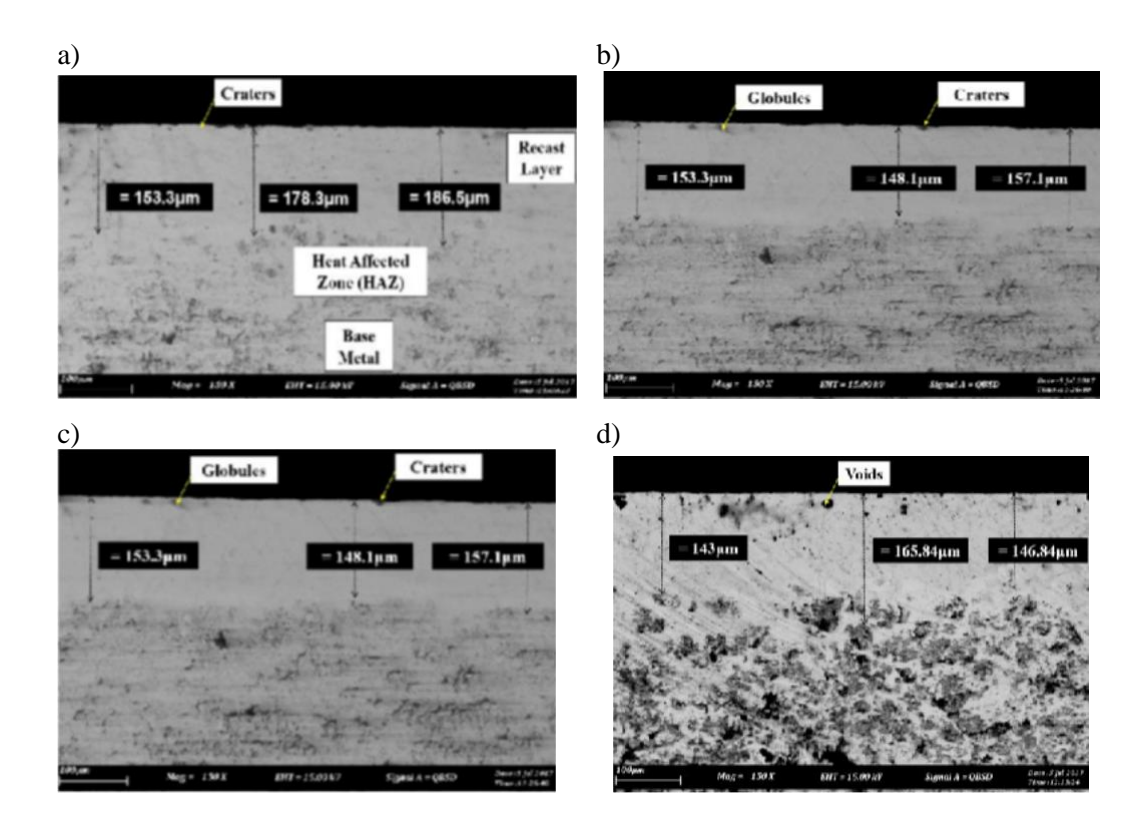


Figure 2: White layer thickness of the studied sample 5 of a) XW42, sample 6 of b) M1, c) M2 and d) enhanced XW42 (M3) WEDM steels

This observation is supported by findings from Karimi Zarchi et al. (2013), who investigated the nitrocarburized surface layer of AISI 1020 in a urea electrolyte, demonstrating similar white layer behaviour. This interpretation aligns with studies by Maher et al. (2015) and Azam et al. (2016), both of which reported that the maximum white layer thickness occurs at the highest levels of peak current and pulse-on time. These machining parameters directly influence the spark energy, thereby increasing the thermal input required to melt or vaporize the workpiece surface.

White layer thickness was found to increase with voltage, a trend further confirmed in the subsequent analysis. This phenomenon is anticipated, as higher voltage levels result in greater spark energy, causing more material to melt and form deeper craters, thus increasing both material removal and heat penetration. Consequently, the formation of a thicker white layer occurs. Najm (2018) also reported that wire tension has a minimal influence on white layer thickness.

Figures 2(b) and 2(c) show nearly identical white layer thickness values of 152.80μm and 152.83μm for M1 and M2, respectively, under identical machining parameters (T<sub>on</sub>: 2μs, V: 6V, WT: 120N). Although the parameters remained constant, the variation in white layer thickness is attributed to differences in alloying composition, where M2 contains niobium and trace amounts (0.005wt%) of cerium and lanthanum. Similarly, Figure 2(d) illustrates a white layer thickness of 151.89μm for enhanced XW42 (M3), machined under the same parameters. Enhanced XW42 (M3) differs in composition by having 0.01wt% of cerium and lanthanum. However, enhanced XW42 (M3) recorded

the lowest white layer thickness (144.32 $\mu$ m) under medium  $T_{on}$ , V, and WT settings, though it exhibited poor surface roughness at 3.54 $\mu$ m.

A comparative microstructural analysis was conducted for Sample 5 (XW42) and Samples 6 (M1, M2, M3). The typical microstructural features shown in Figure 2 highlight the surface characteristics of the recast layer. In high carbon high chromium (HCHCr) steels, the machined surface is generally composed of three distinct zones: the recast layer, the heat-affected zone (HAZ), and the base material (Figure 2(a)). The thickness of these layers is non-uniform and varies with machining conditions. This non-uniformity is primarily due to fluctuations in the spark gap and current instability during the WEDM process. Amorphous regions were observed within the recast layer, formed by resolidified molten material that was not fully removed by flushing. The extremely high thermal gradients, followed by rapid quenching, result in both amorphous and martensitic transformations.

Micro-craters observed in the recast layer (Figures 2(b) and 2(c)) are attributed to localized plasma temperatures exceeding 5000 K. This causes material to melt and partially vaporize. The surface layer evaporates, and the remaining molten material is flushed away by the dielectric fluid, leaving behind crater features with martensitic transformations between martensite plates.

Energy Dispersive X-ray Spectroscopy (EDS) was employed to analyze the elemental composition within the white layer. The technique produces contrast-enhanced images, as shown in Figure 2(d), depicting the white layer microstructure of Sample 6 (M3) under 500× magnification after WEDM. The layer exhibits four distinct phases, characterized by varying contrast: grey phases dominate the upper section, while lighter grey phases appear in the lower region. These variations are likely due to temperature and compositional differences induced by WEDM.

At a low  $T_{on}$  (2µs), low voltage (6V), and high wire tension (120N), the material exhibited the highest material removal rate (MRR) of  $8.11 \times 10^{-3}$ kg. This is attributed to the prolonged pulse-off time, which facilitates better flushing and heat concentration within a narrow spark gap, enhancing erosion efficiency.

## 3.2 Scanning Electron Microscope (SEM) Analysis of Surface Roughness

Figure 3 illustrates SEM images for the machined surfaces of sample 5 (XW42) and sample 6 (M1, M2, and M3). From Figure 3(a), it can be inferred that XW42, processed under conditions of short pulse on time ( $T_{on}$  = 2 $\mu$ s), elevated voltage (10V), and low wire tension (80N), produced shallow craters on the surface. These conditions correspond to a relatively low surface roughness (SR) of 2.07  $\pm$  0.04  $\mu$ m. The formation of a wider plasma channel during discharge and the accumulation of debris within the discharge gap contributed to this effect. Inefficient flushing and the associated high thermal energy led to melting on the workpiece surface.

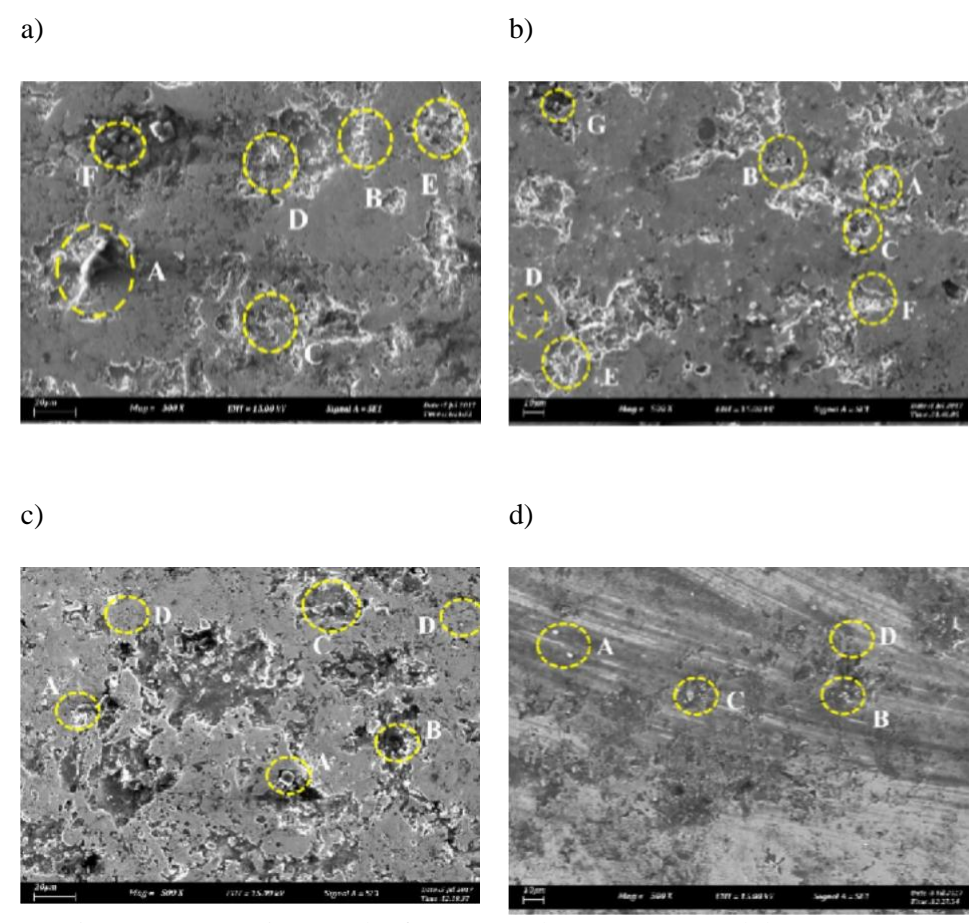


Figure 3: SEM micrograph of a) XW42, b) M1, c) M2 and d) M3 WEDM surface. (Notes: circled structure represent  $M_7C_3$ -A and B, shallow craters-B, shallow craters-C, small gas holes-d and micro-voids -E and wire wear out - F)

Figure 3, parts (a) through (d), visually present SEM micrographs of XW42, M1, M2, and M3, respectively. The images identify various features such as M7C3-type precipitates (labelled A and B), shallow craters (C), gas pores (D), micro-voids (E), and wire electrode debris (F). Gas bubbles, formed during machining and trapped as the melt solidified, as well as molten materials from the eroded wire electrode, contribute to surface irregularities. Not all debris is efficiently flushed out, and some of it redeposits onto the machined surfaces.

Two distinct types of  $M_7C_3$  carbide precipitates were found on the surface, denoted A and B, and verified using X-ray diffraction (XRD) analysis. These carbides manifest as white and silver peaks, indicating their distribution within the grain matrix.

In Figure 3(b), a reduction in surface roughness to  $2.03 \pm 0.06 \mu m$  is observed. This sample was machined with the same  $T_{on}$  (2 $\mu$ s) but lower voltage (6V) and higher wire tension (120N). These changes reduced discharge energy, resulting in smaller craters and a finer surface finish. The WEDM surface shows overlapping shallow craters and some gas holes, formed as entrapped gases escaped during the solidification of re-deposited material. The lower thermal energy also results in a lower presence of molten metals and gas voids. Cracks (D) were observed due to high thermal stresses followed by rapid cooling.

In Figure 3(c), the surface roughness remains similar at  $2.03 \pm 0.07$  µm under identical electrical parameters. Surface analysis revealed signs of brass deposition from the wire electrode and oxidation effects on the workpiece surface, later confirmed through Energy Dispersive X-ray Spectroscopy (EDS) and XRD. Additionally, thermal cracks (B and C) on the surface were identified as detrimental to the recast layer's mechanical integrity.

Figure 3(d) shows the smoothest surface, with a surface roughness of  $1.92 \pm 0.12$  µm. Conditions used include low  $T_{on}$  (2µs), reduced voltage (6V), and high wire tension (120N). These parameters significantly reduced thermal input, resulting in smaller and shallower craters. The density of micro-voids and solidified materials was minimal.  $M_7C_3$  precipitates (A and B) were again observed.

Overall, the experiments demonstrated that sample 5 (XW42) processed under high voltage and low wire tension had the highest surface roughness ( $2.07 \pm 0.04 \mu m$ ), while sample 6 (M3) machined with lower voltage and higher tension yielded the lowest ( $1.92 \pm 0.12 \mu m$ ). Reduced  $T_{on}$  and voltage not only decreased thermal load but also enhanced debris removal due to the longer pulse off time, resulting in a smoother finish.

These findings align with the conclusions drawn by Maher et al. (2016), who reported increased surface roughness at higher discharge energy and longer  $T_{on}$ , leading to larger and deeper craters. Similarly, Manjaiah et al. (2014) confirmed that increased  $T_{on}$  leads to enhanced crater dimensions, thus affecting the final surface texture adversely.

#### 3.3 Optimization factors using full factorial design

The primary objective of optimization is to identify the most effective configuration that satisfies a set of prioritized criteria or constraints. In this study, the aim is to optimize machining parameters to enhance key performance indicators, namely material removal rate (MRR), surface roughness (SR), and white layer thickness (WLT). A full factorial design of experiment (DoE) was employed using a two-level, 2³ factorial design approach. The resulting experimental layout and corresponding machining responses for material enhanced XW42 (M3) are presented in Table 4. According to the data, MRR values ranged from 0.00103kg/s to 0.00821kg/s, SR values varied from 1.92μm to 3.73μm, and WLT measurements spanned from 144.32μm to 340.97μm.

Table 4: Experimental design complete matrix using two level full factorial with effects calculated for enhanced XW42 (M3)

Run	Ton (µs)	V (V)	WT (N)	MRR (kg/s)	SR (µm)	WLT (µm)
1	6	8	100	0.00141	3.47	200.05
2	6	8	100	0.00129	3.54	144.32
3	8	6	120	0.00104	3.62	205.48

4	2	6	80	0.00769	2.03	157.44
5	2	10	80	0.00792	2.08	340.08
6	2	6	120	0.00811	1.92	184.87
7	8	10	120	0.00127	3.62	340.97
8	8	6	80	0.00103	3.39	197.49
9	8	10	80	0.00821	3.73	340.08
10	6	8	100	0.00103	3.33	184.87
11	2	10	120	0.00123	3.16	340.97
12	6	8	100	0.0014	3.55	197.49

# 3.3.1 Surface roughness

The regression equation for SR in terms of coded values is:

$$SR=2.51+0.37A+0.42B+0.18C-0.10AB-0.17AC-0.098BC+0.17A2+0.30B2+0.11C2$$
 where; A= Pulse on time (T<sub>on</sub>); B= Voltage (V); C=Wire tension (WT)

The model summary for Surface Roughness (SR) confirms the statistical significance of the regression model, as indicated by a high F-value of 26.11 and a p-value of less than 0.0001, suggesting the results are not due to chance. The lack of fit test yields an F-value of 0.96 with a p-value of 0.4922, which is not significant, indicating that the model adequately fits the experimental data. The model also demonstrates excellent predictive performance, with an R<sup>2</sup> value of 0.9675, an adjusted R<sup>2</sup> of 0.9429, and a predicted R<sup>2</sup> of 0.8552. Furthermore, the adequate precision value of 17.956, which exceeds the desirable threshold of 4.0, confirms that the model has a strong signal-to-noise ratio and is suitable for use in navigating the design space. This strong model fit suggests reliable predictions for surface roughness based on the three input factors.

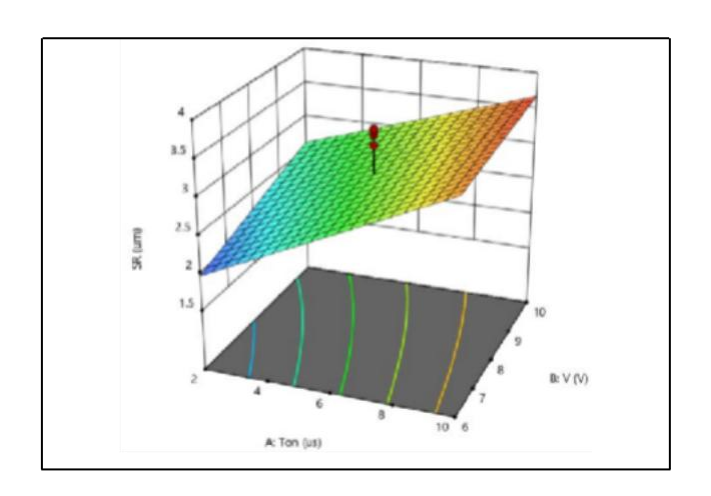


Figure 3: Effect between Ton and V on SR

The 3D surface plot depicts the interaction effect of Pulse-On Time ( $T_{on}$ ) and Voltage (V) on Surface Roughness (SR) in the machining process. The plot shows that both  $T_{on}$  and Voltage contribute to an increase in SR, with surface roughness increasing steadily as  $T_{on}$  increases from 2 to 10 $\mu$ s and Voltage increases from 6 to 10V. The surface forms a rising plane, indicating a strong positive relationship between these parameters and SR. This suggests that higher energy input, resulting from longer  $T_{on}$  and higher Voltage, leads to more aggressive discharges and crater formation, which deteriorates surface quality. The interaction effect is evident, although more linear in nature compared to MRR, showing that the combined effect of  $T_{on}$  and Voltage compounds the roughness. To minimize SR, the process should operate at lower  $T_{on}$  and Voltage settings, reinforcing the importance of optimizing discharge energy to achieve better surface finishes.

# 3.3.2 White Layer Thickness (WLT)

The regression equation for WLT in terms of coded values is:

WLT=6.93+1.58A+1.15B+0.64C-0.67AB-0.22AC-0.26BC+0.25A2+0.51B2+0.

The model summary for White Layer Thickness (WLT) shows that the regression model is statistically significant, with an F-value of 18.67 and a p-value of less than 0.0001, indicating that the results are unlikely due to random variation. The lack of fit is not significant, as evidenced by an F-value of 1.35 and a p-value of 0.3382, suggesting that the model fits the experimental data well. The model also exhibits strong explanatory and predictive capabilities, with an R<sup>2</sup> of 0.9533, an adjusted R<sup>2</sup> of 0.9156, and a predicted R<sup>2</sup> of 0.8071. Additionally, the adequate precision value of 17.053, which is well above the threshold of 4.0, confirms a sufficient signal-to-noise ratio, making the model reliable for exploring the design space.

This model demonstrates that the input factors significantly influence the white layer thickness and that the regression model is robust and predictive.

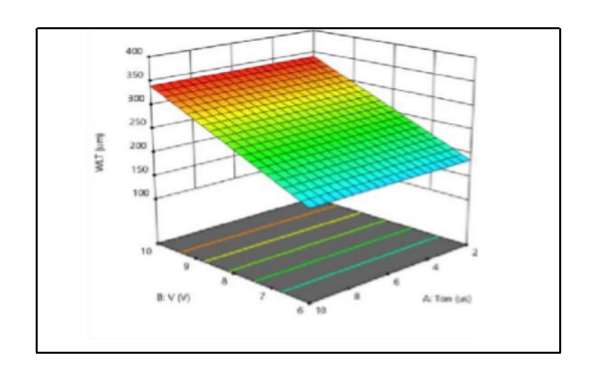


Figure 4 : Effect between Ton and V on WLT

Based on experimental observations, white layer thickness (WLT) exceeding 160µm is considered unsuitable for achieving high-quality surface finishes. Excessive WLT contributes to increased brittleness and a higher likelihood of crack formation, compromising the mechanical integrity and overall performance of the machined component.

## 3.4 Predictive modelling for enhanced XW42 (M3)

Predictive modelling plays a crucial role in forecasting outcomes by analyzing current datasets and identifying underlying trends. In this study, simulation software was employed to develop predictive models for three key parameters: Material Removal Rate (MRR), Surface Roughness (SR), and White Layer Thickness (WLT), using factorial design-based regression. The resulting models are represented by Equations 1 and 2 respectively, with average prediction errors of 0.70% for SR, and 8.2% for WLT.

The surface roughness (SR) model, derived through a two-level factorial analysis, is as follows:

Here, A, B, and C represent the coded levels of the input variables (e.g., Ton, Voltage, and Wire Tension, respectively). The interaction terms (AB, AC, BC, ABC) highlight the combined influence of these parameters.

The model for predicting white layer thickness (WLT) is simpler and is defined as:

$$WLT = 263.42 + 77.10B$$
 (Equation 2)

This implies that WLT is significantly influenced by parameter B (voltage), with a direct and proportional relationship.

The SR model achieved an impressively low average error margin of 0.70%, indicating excellent accuracy and reliability in its predictive capability. The small deviation between the predicted and actual values demonstrates the model's robustness for optimizing surface roughness in the machining of enhanced XW42 (M3). Similarly, the WLT model yielded a prediction error of 8.2%, which is within an acceptable range for industrial processes, confirming that the model is suitable for forecasting and process control.

Comparative analysis with previous research reinforces the validity of this approach. For instance, Maher et al. (2015) achieved an average prediction error of 2.91% for WLT using an adaptive neuro-fuzzy inference system (ANFIS) applied to AISI D2 steel. Likewise, Singh et al. (2014) reported

an SR prediction error below 10% using response surface methodology (RSM), also on AISI D2. These findings support the efficacy of the predictive modelling strategy employed in the present study.

## 4.0 DISCUSSION AND CONCLUSIONS

This study investigates the performance of material enhanced XW42 (M3) during the Wire Electrical Discharge Machining (WEDM) process, focusing on key responses: White Layer Thickness (WLT) and Surface Roughness (SR). The findings show that enhanced XW42 (M3) can achieve a low WLT of 144.32 $\mu$ m under medium settings of pulse-on time (T<sub>on</sub>), voltage (V), and wire tension (WT) (Sample 2). Additionally, enhanced XW42 (M3) demonstrated low SR of 1.92  $\mu$ m at low T<sub>on</sub> and V with high WT (T<sub>on</sub> = 2 $\mu$ s, V = 6V, WT = 120N) in Sample 6.

Microscopic analysis confirmed the absence of surface defects such as micro-cracks, globules, voids, and debris in the recast layer, indicating stable machining conditions for enhanced XW42 (M3). The process optimization was conducted using Full Factorial Design (FFD) with two levels for each of the three factors (Ton, V, WT). ANOVA analysis revealed significant factor contributions. For SR, Ton had the highest influence (64.45%), followed by V (6.41%) and the three-way interaction (5.64%). For WLT, voltage was the most significant factor, contributing 69.23%.

The statistical models developed were validated with high accuracy, showing R<sup>2</sup> values of 99.3% (SR), and 93.5% (WLT), indicating strong predictive capability. The low prediction errors for all three responses further confirm the reliability of the model. The study highlights the importance of selecting materials with balanced hardness and toughness for WEDM, especially in the tool and die industry. It also contributes to the growing research on advanced materials and their compatibility with modern machining technologies. In practical terms, the research supports the need for optimized machining settings to achieve low-cost, high-quality production. The application of FFD ensures efficient process control with minimized sample sizes, reducing time and cost.

## 5.0 ACKNOWLEDGEMENT

This research was partially supported by Universiti Teknikal Malaysia Melaka (UTeM) through the project grant PJP/2017/FKP-AMC/S01560. The authors gratefully acknowledge UTeM for its financial support. Appreciation is also extended to the Advanced Training Centre (ADTEC) Melaka and the National Centre for Machinery and Tool Technology (NCMTT), SIRIM Berhad, Rasa, Selangor, Malaysia, for providing access to the Wire Electrical Discharge Machining (WEDM) equipment and foundry facilities essential to this study.

#### **REFERENCES**

Arif, M., Jahan, M. P., & Saleh, S. (2022). Optimization of wire electrical discharge machining (WEDM) process parameters for improved material removal rate and surface finish. Journal of Manufacturing Processes, 62, 342–355. https://doi.org/10.1016/j.jmapro.2021.11.027

Das, S. R., & Sahoo, A. K. (2023). Multi-objective optimization and predictive modeling of hard milling AISI D2 steel using RSM and NSGA-II. Materials Today: Proceedings, 78, 312–319.

Das, S. R., & Sahoo, P. (2023). Investigations on machining AISI D2 steel by high-speed milling under dry conditions. International Journal of Advanced Manufacturing Technology, 127(3–4), 1123–1135. https://doi.org/10.1007/s00170-023-11528-5

Gautier, A., Lee, J., & Smith, R. (2015). Application of full factorial design in WEDM research. International Journal of Advanced Manufacturing Technology, 85(7–8), 1879–1890. https://doi.org/10.1007/s00170-015-7529-9

Ghodsiyeh, S. M., Moghaddam, H. A., & Jafari, R. (2013). Statistical analysis and optimization of WEDM parameters for material removal rate and surface roughness. Journal of Manufacturing Science and Engineering, 135(5), 051008. https://doi.org/10.1115/1.4025630

Kumar, A., Gupta, R., & Singh, S. (2020). Optimization of WEDM process parameters for material removal rate and surface quality of hardened steels. Journal of Manufacturing Science and Engineering, 142(2), 021012. https://doi.org/10.1115/1.4047772Kumar, N., Saini, N., & Sidhu, S. S. (2022). Influence of WEDM parameters on white layer formation and surface integrity of tool steels: A review. Surface Topography: Metrology and Properties, 10(1), 014001.

Kumar, R., & Verma, A. (2020). Prediction of surface roughness and tool wear using artificial neural networks in hard milling of D2 steel. Journal of Intelligent Manufacturing, 31(6), 1403–1414.

Kumar, R., & Verma, P. (2020). Effect of process parameters on material removal rate and surface finish in WEDM: A review. Journal of Materials Processing Technology, 274, 116359. https://doi.org/10.1016/j.jmatprotec.2019.116359

Ndaliman, M. B. (2022). Hardened steel components and surface integrity in machining: An overview. ScienceDirect. https://www.sciencedirect.com/topics/engineering/hardened-steel

Rosli, M. I., Jamaludin, S. I., & Azuddin, M. H. (2018). Wire electrical discharge machining of tool steels for die and mold applications: A review. Procedia CIRP, 71, 424–429. https://doi.org/10.1016/j.procir.2018.05.084

Rosli, M. N., Jamaludin, S. B., & Azuddin, M. (2018). Performance evaluation and microstructural characteristics of improved tool steel alloy XW42 by WEDM. ResearchGate. https://www.researchgate.net/publication/328184704

Singh, R., & Rao, P. S. (2023). Analysis of white layer formation and its effect on the surface integrity of tool steel in WEDM. Journal of Manufacturing Processes, 87, 23–34.

Singh, R., & Rao, P. S. (2023). Comparative evaluation of ANN and RSM models for WEDM process optimization. Journal of Manufacturing Science and Engineering, 145(2), 021005.

Smith, J., & Lee, H. (2018). Development of custom fixtures for precise alignment in wire EDM. Precision Engineering Journal, 47, 110–118. https://doi.org/10.1016/j.precisioneng.2018.07.012

Sodick. (2020). Sodick AG600L WEDM machine manual. Retrieved from [Sodick official website]

Stat-Ease. (2020). Design Expert software. Retrieved from https://www.statease.com

Tan, Y., & Zhang, W. (2019). Systematic analysis of process variables in wire EDM. Journal of Materials Processing Technology, 267, 9–19. https://doi.org/10.1016/j.jmatprotec.2018.10.021

Tan, Z. (2021). Advancements in wire EDM machines and process control. Journal of Advanced Manufacturing, 35(4), 88–102. https://doi.org/10.1016/j.jam.2020.12.004

Yadav, A., Verma, S., & Jha, P. K. (2023). Optimization of WEDM process parameters using Taguchi- GRA for high-speed tool steel. Materials Today: Proceedings, 78, 352–358.

Yuan, Y., & Zhou, X. (2021). Effect of process parameters on white layer formation in WEDM: A review. Journal of Manufacturing Processes, 62, 97–105. https://doi.org/10.1016/j.jmapro.2021.02.012

Zhang, L., & Zhang, J. (2019). Numerical control and its role in advanced WEDM technologies. International Journal of Advanced Manufacturing Technology, 103(1–4), 45–56. https://doi.org/10.1007/s00170-019-04130-6

Zhang, T., Singh, P. K., & Rao, P. S. (2024). Multi-response optimization of WEDM parameters using hybrid AI models for tool steels. Journal of Manufacturing Processes, 92, 145–158.